International Journal of Heat and Mass Transfer 243 (2025) 126876

Contents lists available at ScienceDirect

International Journal of Heat and Mass Transfer

journal homepage: www.elsevier.com/locate/ijhmt

Method for generating a complete saturated pool boiling curve for cryogenic fluids under terrestrial gravity

Faraz Ahmad [a], Dylan Foster [a], Sunjae Kim [a], Michael Meyer [b], Jason Hartwig [c], Issam Mudawar [a,b,*]

[a] Purdue University Boiling and Two-Phase Flow Laboratory (PU-BTPFL), School of Mechanical Engineering, Purdue University, 585 Purdue Mall, West Lafayette, IN 47907, USA
[b] MTS Inc., 3495 Kent Ave, West Lafayette, IN 47906, USA
[c] NASA Glenn Research Center, Fluids and Cryogenics Branch, Cleveland, OH 44135, USA

ARTICLE INFO

Keywords:
Continuous pool boiling curve
Cryogens
Universal correlations
Terrestrial gravity

ABSTRACT

Constructing a complete and continuous boiling curve is a very challenging endeavor because correlations have historically been developed in individual studies only for specific boiling regimes or transition points, often using different fluids and operating conditions. The present study tackles systematically the complexities of this endeavor by relying on predictive correlations recently developed by the present authors for all individual pool boiling curve regimes and transition points for cryogenic fluids. It is shown how, by integrating the previous correlations and correcting for any discontinuities between correlations, a continuous saturated pool boiling curve can be constructed across the entire range of wall superheats and heat fluxes for all cryogens. The predicted boiling curves are validated against experimental data for key cryogens such as liquid helium, liquid hydrogen, and liquid nitrogen across varying pressure ranges. The critical heat flux is shown to decrease with increasing surface orientation angle, measured from horizontal upward facing, and this effect becomes more pronounced with increasing pressure. The heat transfer coefficient in both the nucleate boiling and film boiling regions increases with increasing pressure, but this trend, especially for nucleate boiling, is less evident at very high pressures. Reinforcing published trends, the decrease in the nucleate boiling heat transfer coefficient near the critical heat flux point is clearly captured, especially for cryogens with relatively high saturation temperatures, such as liquid oxygen and liquid methane. Additionally, the presented methodology shows the wall superheats for the critical heat flux and minimum heat flux points decrease with increasing pressure, excepting very high pressures. Overall, the methodology for generating the complete boiling curve for cryogens is validated over broad pressure ranges, up to 75 % of critical pressure ($p = 0.75p_c$).

1. Introduction

1.1. Significance of thermal management to space applications

In 2024, the Space Technology Mission Directorate (STMD) of National Aeronautics and Space Administration (NASA) conducted a survey to identify 187 technological gaps—key areas needing advancement to support scientific research, future exploration, and other mission objectives. The survey aimed to prioritize the most urgent challenges in the field, helping shape the direction of future space technology innovations and investment strategies. While the majority of the responses (769) came from NASA's internal departments, 462 additional responses were gathered from external stakeholders, including federally funded research institutions, universities, non-profit organizations, professional societies, and other government agencies. The findings were published in a report titled "Civil Space Shortfall Ranking July 2024" [1], highlighting thermal management systems as one of the top areas needing more focus due to increasing demands in space applications.

Researchers worldwide have dedicated significant effort to advancing thermal management techniques to meet the evolving needs of various industries. Among these efforts, Purdue University's Boiling and Two-Phase Flow Laboratory (PU-BTPFL) has been a leading contributor over the past four decades. Using a variety of experimental, theoretical, correlation-based, computational, and machine learning methods, investigators at PU-BTPFL have explored a wide range of

* Corresponding author at: MTS Inc., 3495 Kent Ave, West Lafayette, IN 47906, USA. website: https: //engineering.purdue.edu/BTPFL
E-mail address: mudawar@ecn.purdue.edu (I. Mudawar).

https://doi.org/10.1016/j.ijheatmasstransfer.2025.126876
Received 19 December 2024; Received in revised form 6 February 2025; Accepted 21 February 2025
Available online 3 March 2025

Nomenclature

C	Constant in natural convection correlation [dimensionless]
c_p	Specific heat at constant pressure [J. kg^{-1}. K^{-1}]
g	Earth gravitational acceleration [m. s^{-2}]
h	Heat transfer coefficient [W. m^{-2}. K^{-1}]
h_{fg}	Latent heat of vaporization [J. kg^{-1}]
k	Thermal conductivity [W. m^{-1}. K^{-1}]
L_b	Laplace constant or bubble length [m]; $L_b = \sqrt{\frac{\sigma}{g(\rho_f - \rho_g)}}$
L_x	Characteristic length of heating surface [m]
N	Number of data points used to develop a correlation [dimensionless]
Nu	Nusselt number [dimensionless]
n	Exponent in natural convection correlation [dimensionless]
p	Pressure [N. m^{-2}]
p^*	Reduced pressure; $p^* = \frac{p}{p_c}$ [dimensionless]
p_c	Critical pressure [N. m^{-2}]
Pr	Prandtl number [dimensionless]
q''	Hheat flux [W. m^{-2}]
Ra	Rayleigh number [dimensionless]
Ra_g	Rayleigh number for film boiling based on bubble length L_b [dimensionless]
Ra_L	Rayleigh number for natural convection based on characteristic length L_x [dimensionless]
T_c	Critical temperature [K]
T_{sat}	Saturation temperature of fluid [K]
ΔT_{sat}	Wall superheat [K]; $\Delta T_{sat} = T_w - T_{sat}$
ΔT_{sub}	Liquid subcooling [K]; $\Delta T_{sub} = T_{sat} - T_f$

Greek symbols

α	Percentage of predictions within ±30 % of the data
β	Percentage of predictions within ±50 % of the data
θ	Orientation angle of heating surface [°]
μ	Dynamic viscosity [Pa.s]
ρ	Density [kg.m^{-3}]
σ	Surface tension [N.m^{-1}]
σ_b	Stefan-Boltzmann constant [5.67 × 10^{-8} W/m^2.K^4]
φ	Weighting function used in transition boiling correlation [dimensionless]

Subscripts

CHF	Critical heat flux
Exp	Experimental (measured)
f	Saturated liquid
fb	Film boiling
g	Saturated vapor
l	single phase liquid
min	Minimum heat flux
nb	Nucleate boiling
nc	Natural convection
Pred	Predicted (calculated)
sat	Saturation
sub	Subcooling
tb	Transition boiling
w	Heating wall

Acronyms

CHF	Critical heat flux
FB	Film boiling
HTC	Heat transfer coefficient
LAr	Liquid argon
LCH_4	Liquid methane
LHe	Liquid helium
LH_2	Liquid hydrogen
LN_2	Liquid nitrogen
LO_2	Liquid oxygen
MAE	Mean absolute error
MHF	Minimum heat flux
NASA	National Aeronautics and Space Administration
NB	Nucleate boiling
NC	Natural convection
ONB	Onset of nucleate boiling
PU-BTPFL	Purdue University Boiling and Two-Phase Flow Laboratory
STMD	Space Technology Mission Directorate
TB	Transition boiling

cooling schemes aimed at enhancing heat dissipation. They include capillary [2], pool [3], falling-film [4], channel flow [5,6], micro/mini-channel [7], jet [8], and spray [9], as well as hybrid methods combining the merits of multiple schemes [10,11]. Each technique offers distinct advantages and limitations, with its applicability determined by the specific cooling requirements of different industries.

In many scenarios, pool boiling proves to be an optimal cooling method due to its compact and simple design, low operational costs, and passive functionality. As a result, extensive research has focused on understanding the behaviour of pool boiling under various conditions, leading to the development of models and correlations that accurately predict its performance in numerous applications. However, these predictive tools are predominantly tailored for room-temperature fluids such as water and dielectric coolants. With modern industries, particularly in space exploration, increasingly relying on cryogenic fluids that operate at extremely low temperatures, the effectiveness of these predictive tools is suspect, given the drastic differences between the fluid physics of cryogens and those of room-temperature counterparts. Consequently, applying these tools to cryogenic fluids can lead to highly inaccurate or unreliable results. To address this knowledge gap, new models and correlations need to be developed specifically for cryogenic fluids to enable accurate predictions and efficient thermal management.

Recently, a series of studies conducted jointly by a team from PU-BTPFL, and NASA's Glenn Research Center has culminated in new correlations for cryogenic fluids across the different regions and transition points of the pool boiling curve, including nucleate boiling [12], transition boiling [13], film boiling [14], critical heat flux point (CHF) [15], and minimum heat flux (MHF) point [16]. This study aims to build upon these efforts by integrating the different correlations to construct a complete and continuous boiling curve for cryogenic fluids.

1.2. The boiling curve

In pool boiling experiments, the boiling curve is generated in one of two ways: *heat-flux-controlled* and *temperature-controlled*. Depicted in Fig. 1 (a), a heat-flux-controlled experiment is conducted by gradually increasing the heat flux in small increments, followed each by an adequate waiting period to ensure the attainment of steady state data. Starting with a very low heat flux corresponding to liquid natural convection (NC), increasing the heat flux increases the surface temperature as well as temperature of near-surface liquid until the point of onset of nucleate boiling (ONB) where the nucleation commences. Increasing the heat flux further increases the surface-to-fluid temperature difference (wall superheat), promoting more bubble formation, growth, and departure within the nucleate boiling (NB) region. Approaching the CHF

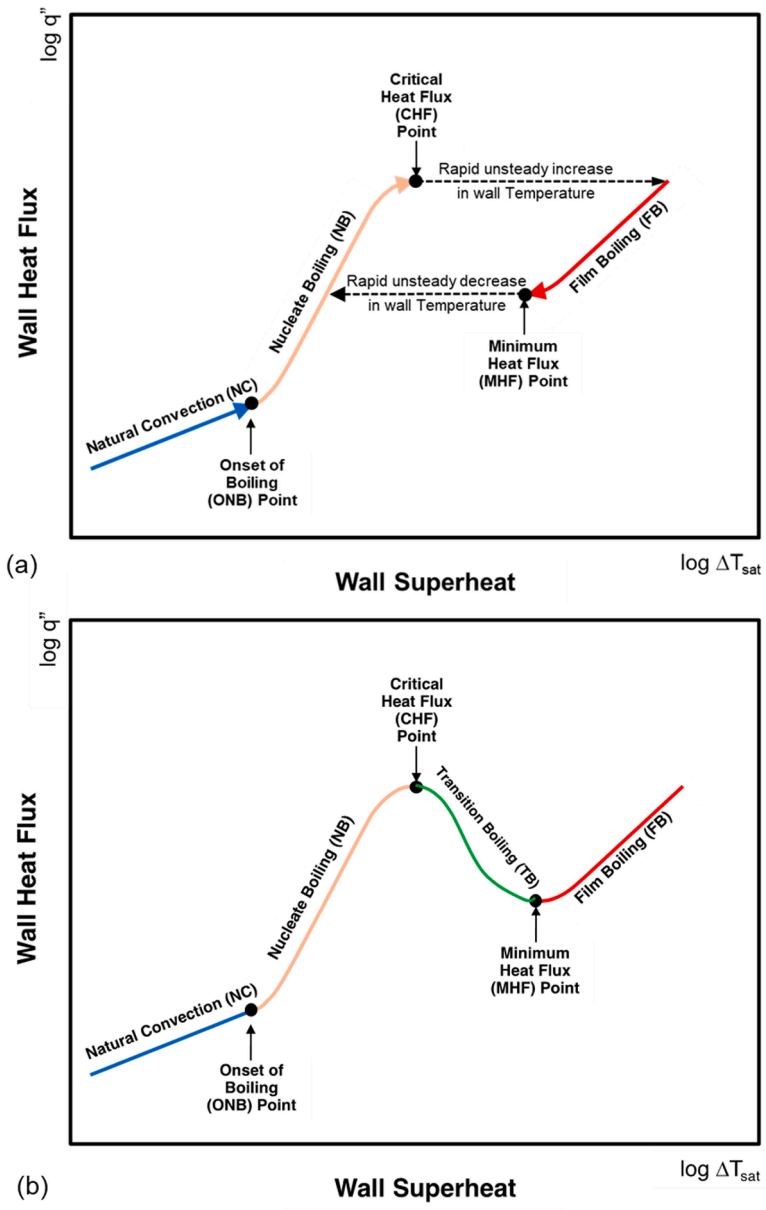

Fig. 1. Boiling curve obtained from (a) heat-flux-controlled experiments and (b) temperature-controlled experiments.

point, effectiveness of the nucleation process diminishes because of appreciable coalescence of large vapor masses which hinder ability of the bulk liquid to replenish the surface. The degradation of nucleate boiling reaches peak value at CHF, at which the surface temperature escalates uncontrollably even while the heat flux stays constant. The surface temperature ceases to rise once film boiling (FB) is reached and any further increase in the heat flux captures the upper region of film boiling. Within FB, the surface is encased in a continuous, thermally insolating vapor layer. Here, heat from the surface must traverse the vapor layer and, given the poor thermal conductivity of the vapor, the heat transfer is highly compromised and the surface temperature attains very high values. Starting from film boiling, the heat-flux-controlled experiment is continued by decreasing the heat flux, once again in small increments. This causes the wall temperature to decrease until reaching the MHF point upon which partial breakup of the vapor layer culminates in a sudden heat transfer enhancement. This is accompanied by a rapid unsteady decline in the surface temperature even while the heat flux stays constant. This allows the system to transition back into the NB region. A further reduction in heat flux brings the system back to the single-phase liquid NC region.

Alternatively, as depicted in Fig. 1 (b), the boiling curve can be generated using a temperature-controlled experiment. In contrast to the heat-flux-controlled experiment, the temperature-controlled experiment sets surface temperature as the primary input, and the system adjusts the heat flux to achieve this target surface temperature. Also, unlike the heat flux-controlled method, the heat flux fluctuates appreciably as the system aims to maintain the desired surface temperature, which renders the experiment quasi-steady rather than perfectly steady-state. This method allows the experiment to proceed by either increasing or decreasing the surface temperature, depending on the choice of the operator. A major advantage of the temperature-controlled method is the ability to capture the transition boiling (TB) region, which cannot be captured in a heat-flux-controlled experiment, thereby generating a complete boiling curve. Overall, despite differences between the two methods, the resulting boiling curves should ideally align except for the TB region, which is only captured by the temperature-controlled experiment.

1.3. Objectives of the present study

In the two-phase heat transfer literature, investigators provide findings from pool boiling experiments conducted under different operating conditions in pursuit of useful correlations. A key challenge when attempting to use such correlations is that most are based on data for room-temperature fluids such is water and dielectric coolants, which is why they are known to yield appreciable predictive errors when applied to the much lower temperature cryogenic fluids. Moreover, correlations from most published works focus are often presented for a specific fluid and more importantly, specific boiling region, often using different assumptions and physical interpretations. This renders the ability to generate a complete boiling curve by stitching together correlations for the different boiling regions from different sources a formidable challenge.

To overcome these challenges, a collaborative effort between PU-BTPFL and NASA Glenn Research Center since 2018 has been focused on generating new correlations that are specific to cryogenic fluids. The ultimate goal of this endeavor is to develop high-accuracy heat transfer correlations to serve as predictive tools for both design and performance assessment of cryogenic systems under different operating conditions and both terrestrial gravity and microgravity. To achieve this goal, over 10,000 datapoints from 80 different papers were amassed and meticulously scrutinized, culminating in 4809 usable data points. These datapoints were first analyzed based on available correlations for mostly room temperature fluids. Based on both useful fluid physics insights from the performance of prior correlations (despite their less than satisfactory predictive accuracy) and the parametric trends from the new cryogenic database, new correlations were developed for NB [12], CHF point surface temperature and heat flux [13,15], TB [13], MHF point temperature and heat flux [16], and FB [14]. It is noteworthy that these initial correlations are intended for only steady-state saturated pool boiling and terrestrial gravity. Effects of other factors, such as microgravity, subcooling, and surface size and material, will be deferred to future work, relying on new cryogenic pool boiling experiments to be conducted in both terrestrial gravity and microgravity. With the new data, the available correlations will be updated, if needed, to broaden their applicability and account for any missing effects. It must be noted that the present study is the first of its kind in terms of generating a complete boiling curve for different cryogens, including liquid helium (LHe), liquid hydrogen (LH_2,) liquid nitrogen (LN_2), liquid argon (LAr), liquid oxygen (LO_2), and liquid methane (LCH_4), under broad ranges of operating conditions.

In summary, the primary objectives of this study are as follows:

i. Summarize previously developed cryogenic correlations for different regions and transition points of the saturated pool boiling curve along with their predictive performance.
ii. Combine the correlations in a MATLAB code wherein fluid, pressure, surface orientation angle, and heat flux are input to calculate the corresponding wall superheat. The complete boiling curve is constructed by combining predictions for all regions and transition points of the pool boiling curve.
iii. Investigate overall shape and trends of the boiling curve and update the correlations where needed. Also, incorporate blending functions where discontinuity in the curve occurs.
iv. Construct final complete and continuous boiling curves for different operating conditions and determine the validity range for the code.
v. Validate the final boiling curves against experimental boiling curves from the literature.

2. Overview of new universal correlations for cryogenic pool boiling

The authors' recent development of new universal cryogenic pool boiling correlations marks a significant step toward understanding cryogenic fluid physics as well as constructing a continuous boiling curve for cryogens. As indicated earlier, the complete boiling curve sought in the present study is intended for flat surfaces in a saturated cryogenic liquid pool and terrestrial gravity, and accounts for variations in pressure, wall heat flux, surface orientation, and the specific cryogen used. To generate a continuous boiling curve by incorporating correlations for the different boiling regions and transition points, further refinement is required. This paper outlines the approach for integrating these correlations to construct a continuous boiling curve. Before delving into the methodology for merging correlations, it is crucial to provide a high-level overview of the key factors and parameters that serve as a foundation for this approach.

2.1. Natural convection (NC)

It is assumed that natural convection in cryogenic fluids follows the same behavior as that for room-temperature fluids. Therefore, a general Nusselt number correlation of the form is used [17]:

$$Nu_{nc} = \frac{h_{nc}L_x}{k_f} = CRa_L^n \tag{1}$$

where h_{nc} is the natural convection HTC [W/m^2.K], L_x the characteristic length of the heating surface [m], k_f the thermal conductivity of single phase liquid [W. m^{-1}. K^{-1}], and Ra_L the Rayleigh number based on characteristic length L_x. The constants C and n depend on both fluid state (laminar or turbulent) and surface orientation [18–21] as summarized in Table 1. Ra_L in Eq. (1) is defined as

$$Ra_L = \frac{L_x^3\rho_f(\rho_f - \rho_{f,w})g}{\mu_f^2}\left(\frac{\mu_f c_{p,f}}{k_f}\right) \tag{2}$$

where ρ_f is the density of single phase liquid calculated at liquid temperature [kg.m^{-3}], $\rho_{f,w}$ the density of single phase liquid calculated at wall temperature [kg.m^{-3}], μ_f the dynamic viscosity of single phase liquid [Pa. s], g the Earth gravity [9.8 m.s^{-2}], and $c_{p,f}$ the specific heat of single phase liquid [J.kg^{-1}.K^{-1}].

2.2. Nucleate boiling (NB)

After meeting the requirements for ONB condition ($\Delta T_{sat} = \Delta T_{sat,ONB}$, $q'' = q''_{ONB}$), bubble nucleation commences and intensifies along the NB region until the CHF condition is met. Heat transfer in NB region can be determined using our recently developed correlation [12],

$$h_{nb} = 13.3\, q''^{0.665}(1 + 0.52\, p^*)^{4.7} Pr_f^{-1.09} \times \left[\frac{1 + 68e^{20(p^*-1.1)}}{1 + 0.0045\, e^{\left(q'' \times 10^{-5}\right)}}\right] \tag{3}$$

where h_{nb} is the NB HTC [W/m^2.K], p^* the reduced pressure (p/p_{crit}), q'' the heat flux [W/m^2], and Pr_f the liquid Prandtl number. Details

Table 1
Summary of values of C and n in natural convection correlations.

Orientation angle [°]	C	n	Validity range	Reference
$\theta = 0°$	0.54	1/4	$10^4 \le Ra_L \le 10^7$, $Pr_L \ge 0.7$	Lloyd & Moran [18]
	0.15	1/3	$10^7 \le Ra_L \le 10^{11}$	Lloyd & Moran [18]
$\theta = 90°$	0.59	1/4	$10^4 \le Ra_L \le 10^9$	McAdams [19]
	0.10	1/3	$10^9 \le Ra_L \le 10^{13}$	Bayley [20]
$\theta = 180°$	0.52	1/5	$10^4 \le Ra_L \le 10^9$, $Pr_L \ge 0.7$	Radziemska & Lewandowski [21]

concerning both the development of this correlation and its predictive performance for different cryogens are provided in [12].

2.3. Onset of nucleate boiling (ONB) point

The ONB point is identified by conditions leading to formation of the first bubble on the heating surface. It is identified on the boiling curve via corresponding values of heat flux, q''_{ONB}, and wall superheat, $\Delta T_{sat,ONB}$. Ideally, while the ONB point falls directly on the boiling curve's NC line, a blending function is required to avoid any discontinuity between the ONB point and NB curve. However, the authors' thorough investigation of published cryogenic pool boiling literature identified two main difficulties in developing an accurate correlation for ONB: (i) sparsity of ONB datapoint for different cryogens, and (ii) for available data, very low values of q''_{ONB} and ΔT_{ONB} are often within the range of measurement uncertainties. To avoid this complication, the ONB point is identified in this study as the intersection of NC and NB correlations, i.e., by setting $(\Delta T_{sat,nc},\ q''_{nc}) = (\Delta T_{sat,nb}, q''_{nb})$.

2.4. Critical heat flux (CHF) and wall temperature ($T_{w,CHF}$)

The CHF point is identified on the boiling curve by corresponding values for both heat flux, q''_{CHF}, and wall superheat, ΔT_{CHF}. Our team's correlation for q''_{CHF} was developed in [15], which can be presented as

$$q''_{CHF} = \left[0.16 - 0.104\ (p^*)^{10}\right] \times \left[1 - 0.004(p^*)\theta\right]\left|\cos\left(\left(\frac{88}{180}\right)\theta\right)\right|^{0.364} \times \left[1 + 0.16\left(\frac{c_{p,f}\Delta T_{sub}}{h_{fg}}\right)\right] \times \left[\rho_g h_{fg}\left(\frac{\sigma g(\rho_f - \rho_g)}{\rho_g^2}\right)^{\frac{1}{4}}\right] \tag{4}$$

where θ is the orientation angle of the heating surface [°], h_{fg} the latent heat of vaporization [J.kg^{-1}], ΔT_{sub} the degree of subcooling of liquid pool [K], whose value is zero for the present saturated pool boiling study, and σ the surface tension of the fluid [N.m^{-1}].

Similarly, a correlation of the CHF point wall temperature, $T_{w,CHF}$, was presented in our recent paper [13] as a function of the MHF point wall temperature, $T_{w,min}$,

$$T_{w,CHF} = 0.775\ T_{w,min} \tag{5}$$

Here, $T_{w,min}$ is calculated using our recently published correlation [16]

$$T_{w,min} = T_{sat} + (T_c - T_{sat})\left(-9.1 + 12\left(\frac{k_f \rho_f c_{p,f}}{k_w \rho_w c_{p,w}}\right)^{0.025}\right) \tag{6}$$

where T_{sat} is the saturation temperature and T_c the fluid's critical temperature, with all temperatures in Eqs. (5) and (6) are expressed in K. The subscripts f and w in Eq. (6) represent fluid and heating surface material, respectively.

These correlations were validated, and showed very good predictions, against mostly lower pressure data (because of the lack of higher-pressure cryogen data). However, a problem arises when attempting to construct the complete boiling curve, caused by the fact that the value of T_{min} decreases with increasing pressure and, above a certain pressure value, shifts the predicted value of T_{CHF} to the left side of nucleate boiling curve, which is physically inconsistent. This problem was circumvented by using a different method wherein T_{CHF} is determined by the intersection of NB curve and q''_{CHF}. Mathematically, this can be represented as

$$\Delta T_{sat,CHF} = T_{w,CHF} - T_{sat} = \frac{q''_{CHF}}{h_{CHF}} \tag{7}$$

where h_{CHF} is the HTC at the CHF point, which is calculated by combining Eqs. (3) and (4),

$$h_{CHF} = 13.3\ (q''_{CHF})^{0.665}(1 + 0.52\,p^*)^{4.7} Pr_f^{-1.09} \times \left[\frac{1 + 68e^{20(p^*-1.1)}}{1 + 0.0045\ e^{\left(q''_{CHF} \times 10^{-5}\right)}}\right] \tag{8}$$

Here, q''_{CHF} is calculated using Eq. (4), marking the upper limit of NB.

2.5. Minimum heat flux (MHF) and wall temperature ($T_{w,min}$)

The MHF point separates the TB region from the FB region. Since the correlation for TB, as discussed in the next section, depends on both the CHF and MHF points, it is necessary to present correlations for the MHF point before those for TB. A detailed description for predicting the MHF point is provided in authors' recent paper [16], where $q''_{\min}$ and ΔT_{min} are determined as follows.

$$q''_{\min} = 0.043\left[\frac{c_{p,g}k_g^2}{\mu_g}\rho_g g(\rho_f - \rho_g)\right]^{0.567} \times \left(-0.107 + 0.38\left(\Delta T_{sat,\min}\right)^{0.39}\right)^{3.094} \tag{9}$$

where μ_g is the dynamic viscosity of saturated vapor [Pa.s], k_g the thermal conductivity of saturated vapor [W. m^{-1}. K^{-1}], $c_{p,g}$ the specific heat of saturated vapor [J.kg^{-1}.K^{-1}], and $\Delta T_{sat,min}$ the wall superheat at the MHF point, which is expressed as

$$\Delta T_{sat,min} = T_{w,min} - T_{sat} \tag{10}$$

where $T_{w,min}$ is calculated using Eq. (6).

2.6. Transition boiling (TB)

Compared to the other boiling curve regimes, TB has received far less attention in the heat transfer literature. A detailed discussion about the few available prior correlations, their performance, and physics of TB can be found in our recent paper [13]. The same study showed a new systematic method for determining the TB curve. First, the wall superheat in TB is given by

$$\Delta T_{sat,tb} = \left[\Delta T_{sat,CHF} + \varphi\ \left(\Delta T_{sat,min} - \Delta T_{sat,CHF}\right)\right] \tag{11}$$

where $\Delta T_{sat,tb}$ is the wall superheat [K] in TB, $\Delta T_{sat,min}$ and $\Delta T_{sat,CHF}$ are the wall superheats [K] at the MHF and CHF points, which can be calculated using Eqs. (10) and (7), respectively, and φ is a weighting function based on both the CHF to MHF points.

$$\varphi = \left|\left(\frac{q''_{tb} - q''_{CHF}}{q''_{min} - q''_{CHF}}\right)^{0.8}\right| \tag{12}$$

where q''_{tb} is the input heat flux [W. m^{-2}] in the TB region, and q''_{CHF}, $q''_{\min}$, and $T_{w,min}$ are calculated using Eqs. (4), (9), and (6), respectively.

An expression for the HTC in TB can be formulated using $h_{tb} = q''_{tb}/(T_{w,tb} - T_{sat})$, which yields

$$h_{tb} = \frac{q''_{tb}}{\left[\left(T_{w,CHF} - T_{sat}\right) + \left|\left(\frac{q''_{tb} - q''_{CHF}}{q''_{\min} - q''_{CHF}}\right)^{0.8}\right|\left\{\left(T_{w,\min} - T_{sat}\right) - \left(T_{w,CHF} - T_{sat}\right)\right\}\right]} \tag{13}$$

2.7. Film boiling (FB)

FB is the highest temperature regime of pool boiling, where high surface temperature causes bubble nucleation to fully subside, replaced by formation of continuous vapor blanket. A detailed description of this regime and its characteristics can be found in our recently published paper [14]. In the same study, the following new HTC correlation was derived from available cryogenic fluid data:

$$h_{fb} = (0.148 + 0.052\sin\theta) \times \frac{k_g}{L_b}\left[Ra_g \cdot \left(\frac{h_{fg} + 0.46\, c_{p,g}\left(T_{w,fb} - T_{sat}\right)}{c_{p,g}\left(T_{w,fb} - T_{sat}\right)}\right)\right]^{0.33} + \frac{(1.7 - 0.55\sin\theta)\,\sigma_b\left(T_{w,fb}^4 - T_{sat}^4\right)}{\left(T_{w,fb} - T_{sat}\right)} \quad (14)$$

where h_{fb} is the *overall* FB HTC [W/m^2.K], accounting for both film boiling and radiation effects, θ the surface orientation angle measured from horizontal upward position [°], h_{fg} the latent heat of vaporization [J/kg], $T_{w,fb}$ the temperature of the heating surface in FB [K], and σ_b the Stefan-Boltzmann constant, 5.67 × 10^{-8} W/m^2.K^4. In Eq. (14), L_b represents the Laplace constant or bubble length [m] which can be calculated using the below equation.

$$L_b = \sqrt{\frac{\sigma}{g(\rho_f - \rho_g)}} \quad (15)$$

Moreover, Ra_g is the Rayleigh number of saturated vapor, which can be determined as

$$Ra_g = \frac{L_b^3 \rho_g (\rho_f - \rho_g) g}{\mu_g^2}\left(\frac{\mu_g c_{p,g}}{k_g}\right) \quad (16)$$

2.8. Blending function between film boiling (FB) and minimum heat flux (MHF) point

It is important to note that, as indicated in our prior work, that the above correlations provide accurate predictions for cryogens when applied to individual boiling curve regions and transition points. However, problems arise when combining these correlations to generate a complete boiling curve. This is reflected by a discontinuity when patching together the heat flux correlations for TB and FB at $q''_{\min}$. An example of such discontinuity is shown in Fig. 2 (a) for LH_2 at a reduced pressure of $p^* = 0.1$. Guided by insights from experimentally available pool boiling curves, the discontinuity is corrected by devising a "blending function" between FB and MHF point, which, as shown later, proved highly effective at predicting boiling curve trends for different cryogens. Through iteration in pursuit of best predictions, an upper heat flux value for the blending function was set at $1.5q''_{\min}$ and, as illustrated in Fig. 2 (b), the blending function is given by

$$\Delta T_{sat,blend} = \Delta T_{sat,min} + \left|\frac{q'' - q''_{\min}}{0.5q''_{\min}}\right|^{0.5}\left(\Delta T_{sat,fb}\big|_{1.5q''_{\min}} - \Delta T_{sat,min}\right) \quad (17)$$

which is applied only in the range of

$$\Delta T_{sat,min} \le \Delta T_{sat} \le \Delta T_{sat,fb}\big|_{1.5q''_{\min}} \quad (18)$$

For the sake of completeness and brevity, a complete summary of all the correlations used to construct the boiling curve, along with application range for each, is provided in Table 2.

3. Performance assessment and validation of correlations used to construct saturated pool boiling curve for cryogens

3.1. Performance summary of developed correlations

Our recently developed correlations for saturated pool boiling of cryogens have already been discussed in the previous section. Further details on each correlation are explained in their respective original papers [12–14,16]. However, to provide a comprehensive overview, this section summarizes the performance for all the developed correlations. The predictive performance is evaluated via four metrics: mean absolute error (MAE), number of data points used in the development of each correlation (N), and percentage of data that are predicted within ±30 % (α) and ±50 % (β). This comparative analysis, presented in Fig. 3 and Table 3, offers a clear perspective on the effectiveness of each correlation across various datasets.

As shown in Fig. 3, based on availability of published data, far more datapoints were employed for developing the NB and FB correlations compared to those for other boiling curve regimes and transition points. Overall, the correlations show very good predictions for multiple cryogens. Notably, the $T_{w,min}$ correlation has an 8.73 % MAE for $N = 165$ data

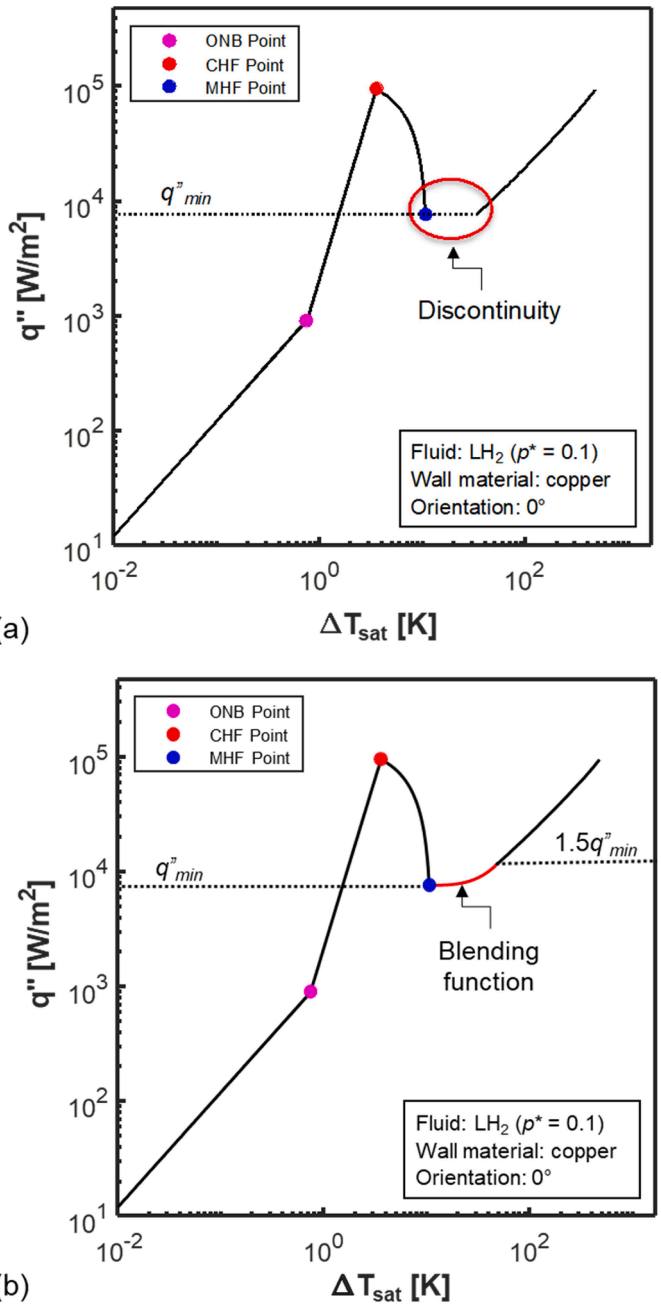

Fig. 2. Complete boiling curve for LH_2 (a) without blending function and (b) with blending function.

Table 2
Summary of correlations used to construct a complete saturated pool boiling curve ($\Delta T_{sub} = 0$) for cryogens.

Reference (s)	Region/Point	Correlation(s)	Application Range	Remarks
[17–21]	Natural convection (NC) region	$h_{nc} = \frac{k_f}{L_x} C Ra_L^n$ $Ra_L = \frac{L_x^3 \rho_f (\rho_f - \rho_{f,w}) g}{\mu_f^2} \left(\frac{\mu_f c_{p,f}}{k_f}\right)$	$\Delta T_{sat} \leq \Delta T_{sat,ONB}$	Values for C and n are provided in Table 1
-	Onset of nucleate boiling (ONB) point	-	$\Delta T_{sat} = \Delta T_{sat,ONB}$	Intersection point of NC and NB
[12]	Nucleate boiling (NB) region	$h_{nb} = 13.3\, q''^{0.665} (1 + 0.52\, p^*)^{4.7} Pr_f^{-1.09} \times \left[\frac{1 + 68 e^{20(p^* - 1.1)}}{1 + 0.0045\, e^{(q'' \times 10^{-5})}}\right]$	$\Delta T_{sat,ONB} < \Delta T_{sat} < \Delta T_{sat,CHF}$	
[13]	Critical heat flux (CHF) point	$\Delta T_{sat,CHF} = T_{sat,CHF} - T_{sat} = \frac{q''_{CHF}}{h_{CHF}}$	$\Delta T_{sat} = \Delta T_{sat,CHF}$	
[15]		$q''_{CHF} = [0.16 - 0.104\, (p^*)^{10}] \times [1 - 0.004(p^*)\theta] \left\|\cos\left(\left(\frac{88}{180}\right)\theta\right)\right\|^{0.364} \times \left[1 + 0.16\left(\frac{c_{p,f}\Delta T_{sub}}{h_{fg}}\right)\right] \times \left[\rho_g h_{fg}\left(\frac{\sigma g(\rho_f - \rho_g)}{\rho_g^2}\right)^{\frac{1}{4}}\right]$		
[13]	Transition boiling (TB) region	$\Delta T_{sat,tb} = [\Delta T_{sat,CHF} + \varphi\, (\Delta T_{sat,min} - \Delta T_{sat,CHF})]$ $\varphi = \left\|\left(\frac{q'' - q''_{CHF}}{q''_{min} - q''_{CHF}}\right)^{0.8}\right\|$	$\Delta T_{sat,CHF} \leq \Delta T_{sat} \leq \Delta T_{sat,min}$	Accuracy of this correlation is strongly dependent on predictions of the CHF and MHF points
[16]	Minimum heat flux (MHF) point	$T_{w,min} = \left[T_{sat} + (T_c - T_{sat})\left(-9.1 + 12\left(\frac{k_f \rho_f c_{p,f}}{k_w \rho_w c_{p,w}}\right)^{0.025}\right)\right]$	$\Delta T_{sat} = \Delta T_{sat,min}$	This correlation accounts for surface material effect
[16]		$q''_{\min} = 0.043 \left[\frac{c_{p,g} k_g^2}{\mu_g} \rho_g g (\rho_f - \rho_g)\right]^{0.567} \times (-0.107 + 0.38\, (\Delta T_{sat,\min})^{0.39})^{3.094}$		This correlation is dependent on $\Delta T_{sat,min}$ correlation
-	Blending function between q''_{min} and $1.5q''_{min}$	$\Delta T_{blend} = \Delta T_{sat,\min} + \left\|\frac{q'' - q''_{\min}}{0.5 q''_{\min}}\right\|^{0.5} \times \left(\Delta T_{sat,fb}\big\|_{1.5q''_{\min}} - \Delta T_{sat,\min}\right)$	$\Delta T_{sat,min} \leq \Delta T_{sat} \leq \Delta T_{sat,fb}\big\|_{1.5q''_{min}}$	FB correlation is terminated at $1.5q''_{min}$ and the blending function is used to merge the FB curve with the MHF point
[14]	Film boiling (FB) region	$h_{fb} = (0.148 + 0.052 \sin\theta) \times \frac{k_g}{L_b}\left[Ra_g \cdot \left(\frac{h_{fg} + 0.46\, c_{p,g}\, (T_{w,fb} - T_{sat})}{c_{p,g}\, (T_{w,fb} - T_{sat})}\right)\right]^{0.33} + \frac{(1.7 - 0.55 \sin\theta)\, \sigma_b \left(T_{w,fb}^4 - T_{sat}^4\right)}{(T_{w,fb} - T_{sat})}$	$\Delta T_{sat} \geq \Delta T_{sat,fb}\big\|_{1.5q''_{min}}$	Correlation also accounts for radiation effects

points, followed by the $T_{w,CHF}$ correlation, 10.71 % for $N = 236$, h_{fb} correlation, 12.94 % for $N = 1209$, h_{tb} correlation, 14.84 % for $N = 133$, q''_{min} correlation, 22.42 % for $N = 158$, and h_{nb} correlation, 25.36 % for $N = 2908$. Notice that certain correlations are evaluated against more cryogens than others; this again is based entirely on the availability of data for a given boiling regime or transition points.

3.2. Validation of new methodology for constructing complete pool boiling curve

While each individual correlation has been thoroughly tested against its respective datasets, Fig. 3, it is crucial to validate the complete boiling curve against experimental data to illustrate the robustness and reliability of the new methodology for the construction of complete boiling curve. Such validation is a key step toward demonstrating practical applicability of the methodology across different cryogens and operating conditions. To this end, the validation is conducted using data for the three most significant and widely used cryogens in scientific and industrial applications: liquid nitrogen (LN_2), liquid hydrogen (LH_2), and liquid helium (LHe).

Ideally, one should aim to validate the entire boiling curve against experimental data from a single source. This would provide a direct comparison between the predicted boiling curve and experimental results across all boiling regimes for same operating conditions. Unfortunately, such comprehensive datasets are very rare in published literature since pool boiling experiments are typically conducted by different researchers, each focusing on specific regime and operating conditions based on their own research objectives. As a result, it is difficult to find a single source of experimental data covering the entire boiling curve.

To address this shortcoming, we took data from different studies, each focused on a particular boiling regime for same cryogen, which are then combined to validate the methodology. This allows validation across multiple datasets, which demonstrates broad applicability of the methodology. For example, Fig. 4 shows the validation for LHe using experimental data from five different sources [22–26] at a pressure of 101 kPa. The results demonstrate very good capability in predicting the LHe data, which include both horizontal and vertical surfaces. Validation of correlations for the ONB, CHF and MHF points is deferred to a later section.

However, some discrepancies arise in the natural convection regime, where predictions show some deviations from the data. This divergence is attributed to several factors. First and foremost is experimental uncertainty, particularly at extremely low temperatures. For LHe, wall superheat can be as low as 0.01 K, which would greatly accentuate measurement uncertainties. Another contributing factor could be limitations of the natural convection correlations used. These correlations were originally developed for mostly room-temperature fluids, and their applicability at such low temperatures may be somewhat compromised. Moreover, as shown in Fig. 4 (b), the validation for natural convection over vertical surfaces for LHe is incomplete due to a lack of corresponding experimental data. This data shortfall highlights the need for further experimental studies, particularly for cryogens like LHe, to provide a more comprehensive database that covers all boiling regimes, including natural convection, over a range of surface orientations.

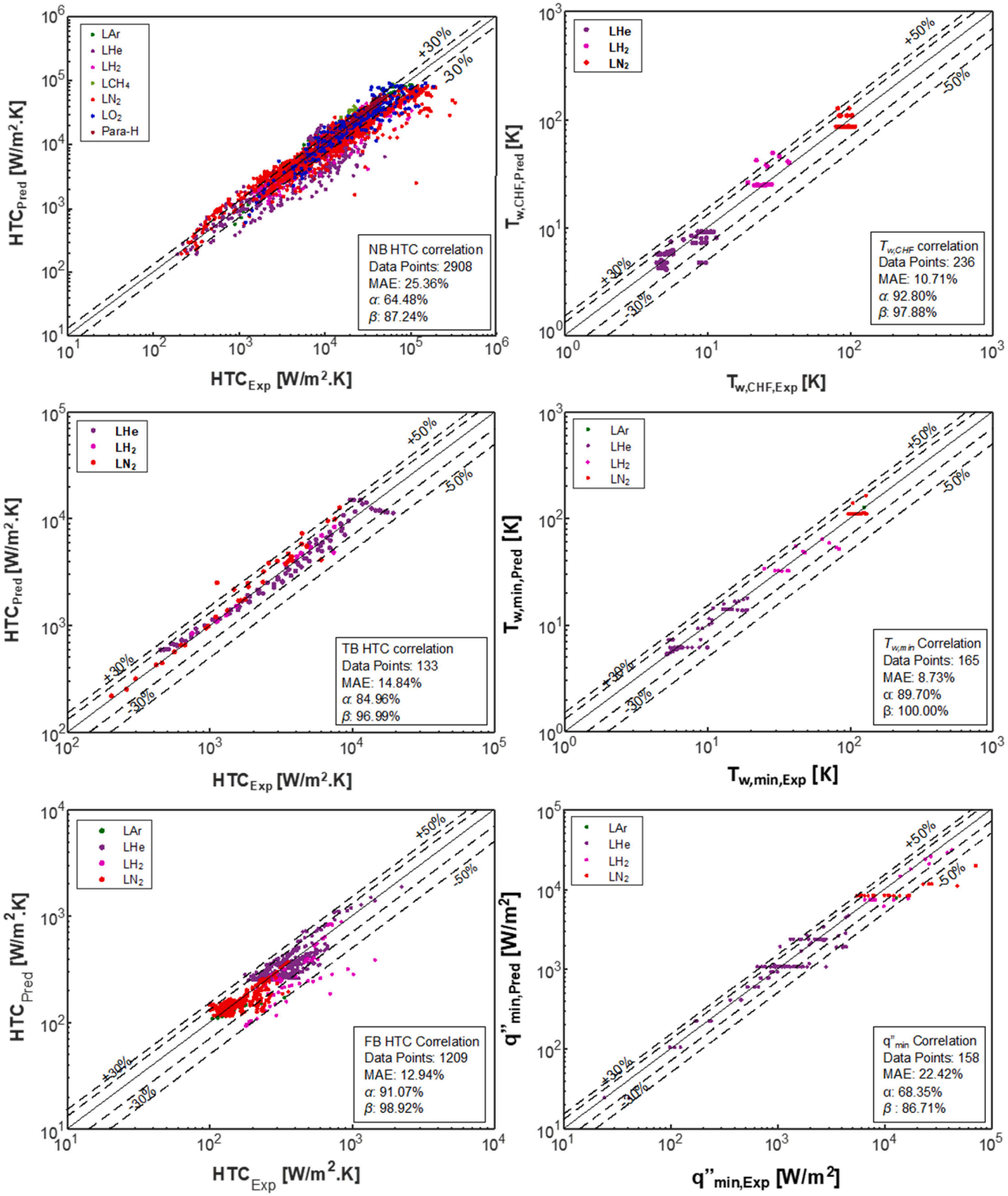

Fig. 3. Performance summary of the cryogenic pool boiling heat transfer correlations.

For LHe, we were fortunate to locate experimental data for all boiling regimes at the same pressure, even though the data came from different sources. This facilitated both complete and consistent validation of the new methodology for LHe. Unfortunately, the same was not possible for other cryogens, as data available for different regimes often came from experiments conducted at different pressures. To address this shortcoming, we opted to collect data spanning a small pressure range rather than a single pressure value.

For instance, Fig. 5 illustrates the validation of the new methodology for LH_2 using data from two different sources [27,28] at somewhat close but unequal pressures, 91 versus 102 kPa. To avoid ambiguity in plotting boiling curves for two distinct pressures on the same graph, the

Table 3
Performance summary of the previously developed PU-BTPFL correlations against cryogenic fluid data.

Correlation	MAE	Number of Data Points, N	Reference
h_{nb}	25.36 %	2908	Ahmad et al. [12]
h_{fb}	12.94 %	1209	Ahmad et al. [14]
h_{tb}	14.84 %	133	Ahmad et al. [13]
q''_{CHF}	16.95 %	1188	Patel et al. [15]
$T_{w,CHF}$	10.71 %	236	Ahmad et al. [13]
$q''_{\min}$	22.42 %	158	Ahmad et al. [16]
$T_{w,min}$	8.73 %	165	Ahmad et al. [16]

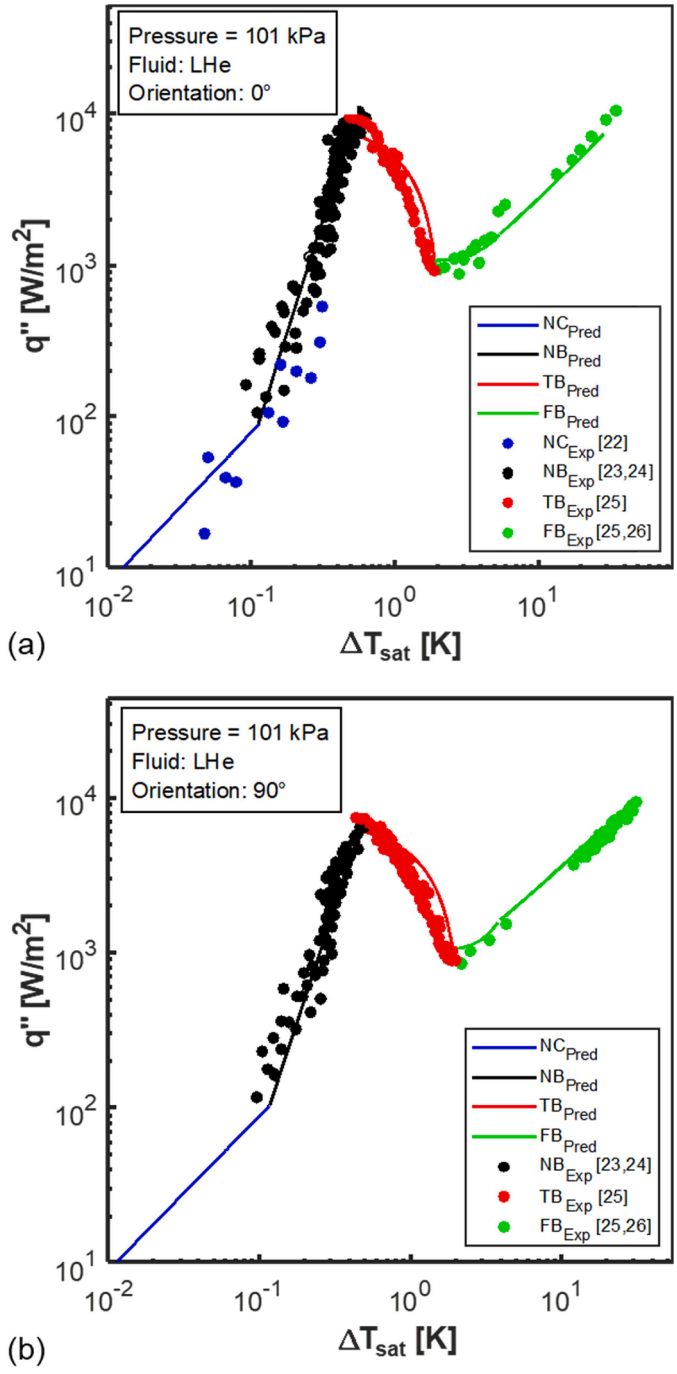

Fig. 4. Validation of new pool boiling curve construction methodology against LHe data for (a) horizontal and (b) vertical surface orientations.

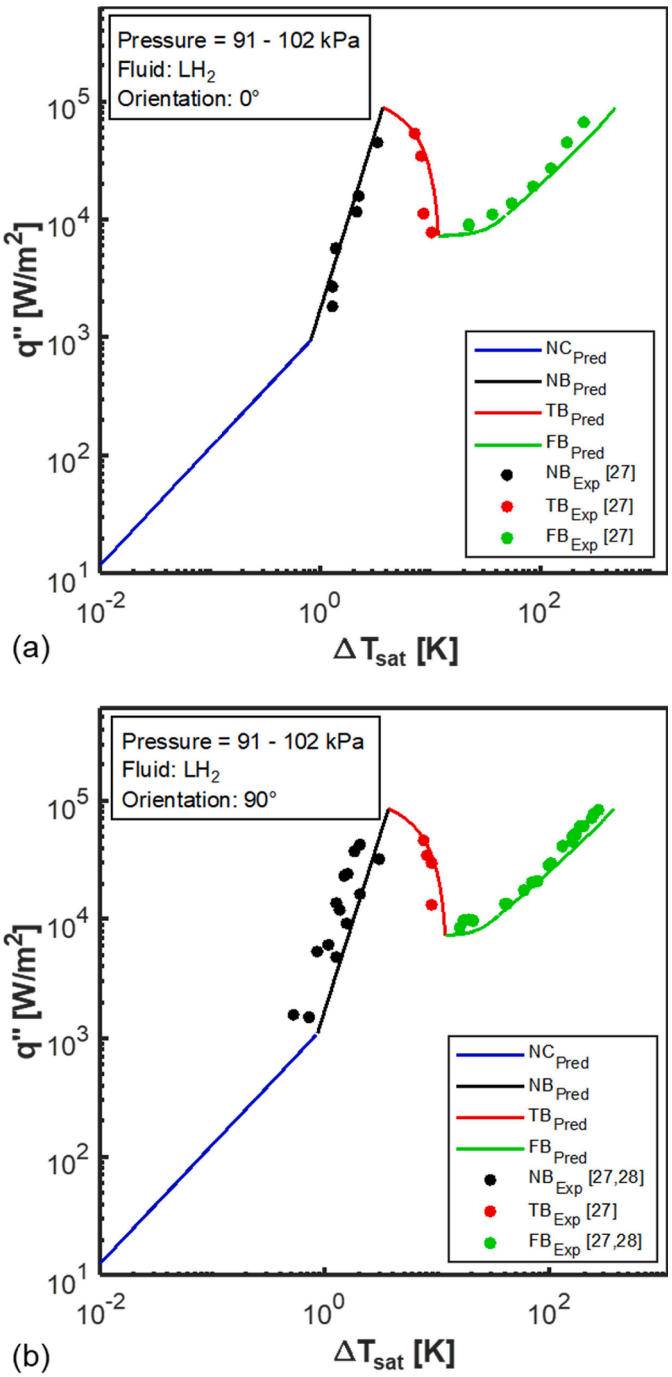

Fig. 5. Validation of new pool boiling curve construction methodology against LH_2 data.

predictions are made for an intermediate pressure of 100 kPa, while noting the range of experimental pressures (91–102 kPa). Fig. 5 show very good alignment of predictions against experimental data across the NB, TB, and FM regions. However, natural convection was not validated because of absence of experimental data for LH_2 in this regime.

Similarly, the present methodology is validated in Fig. 6 against LN_2 data gathered from multiple sources [27,29–32], with a pressure range from 98 to 101 kPa. Here too, predictions based on an intermediate pressure of 100 kPa show good ability in predicting the data for LN_2, which has appreciably higher saturation temperatures compared to those for LHe and LH_2. This suggests that, despite some deviations in both the NC and NB boiling regions, the methodology is effective for both low temperature cryogens (e.g., LHe) as well as higher temperature

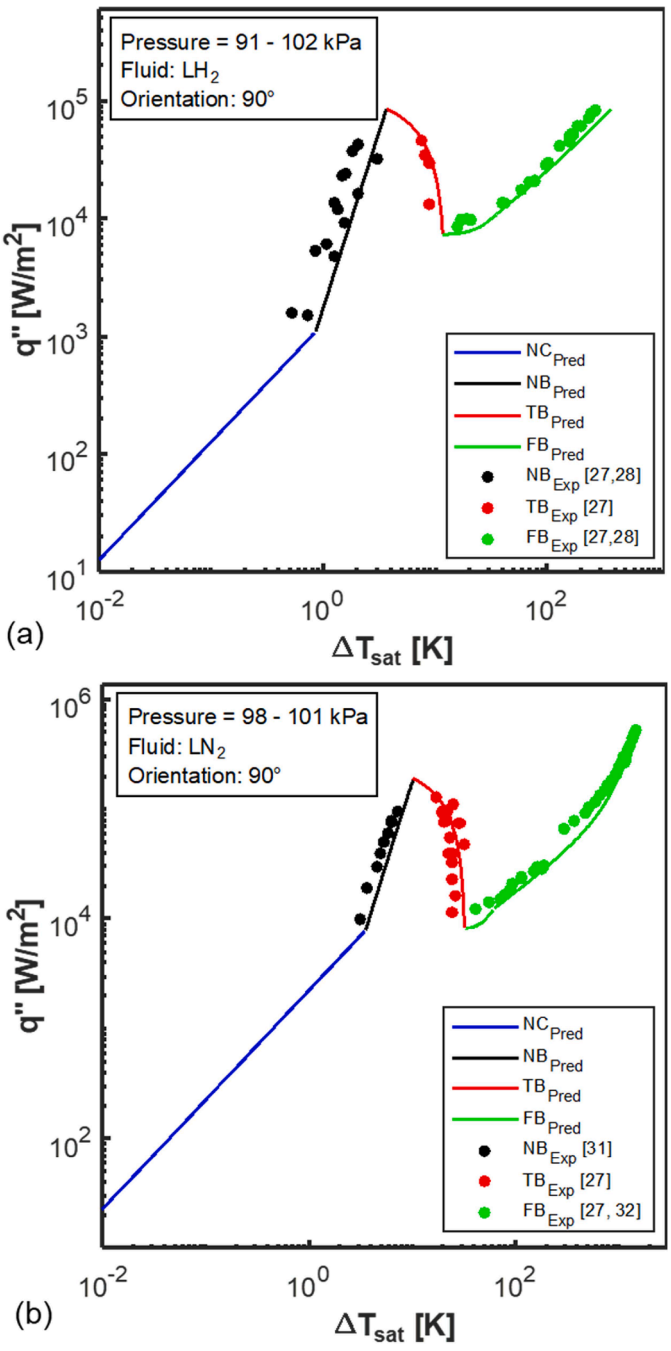

Fig. 6. Validation of new pool boiling curve construction methodology against LN_2 data for (a) horizontal and (b) vertical surface orientations.

(e.g., LN_2, LO_2, and LAr). Note, however, that the deviations manifest in Fig. 6 (a) for NB are artificially magnified by the logarithmic presentation used, since the actual temperature deviations are less than 3°C. However, more appreciable deviations are evident for NC for reasons similar to those presented above for LHe. Moreover, no comparisons are provided for NC in Fig. 6 (b) because of absence of NC data for the vertical orientation.

In conclusion, the new methodology for predicting the complete pool boiling curve shows good overall agreement with the experimental data for LHe, LH_2, and LN_2. This robust performance suggests that the model is likely equally effective for other cryogens as well, as each regime-specific correlation has already been individually validated. However, further work is needed to improve predictive performance, particularly for NC and vertical surface orientation, where experimental data are sparse.

4. Predictions of the continuous saturated pool boiling curve using the new methodology

4.1. Heat-flux-controlled versus and temperature-controlled boiling curves

Before delving into further details of the proposed new methodology, it is prudent to address the differences discussed earlier between steady-state boiling curves measured using heat-flux-controlled and temperature-controlled experiments. Shown in Figs. 7(a) and 7(b) are predicted heat-flux-controlled pool boiling curve and temperature-

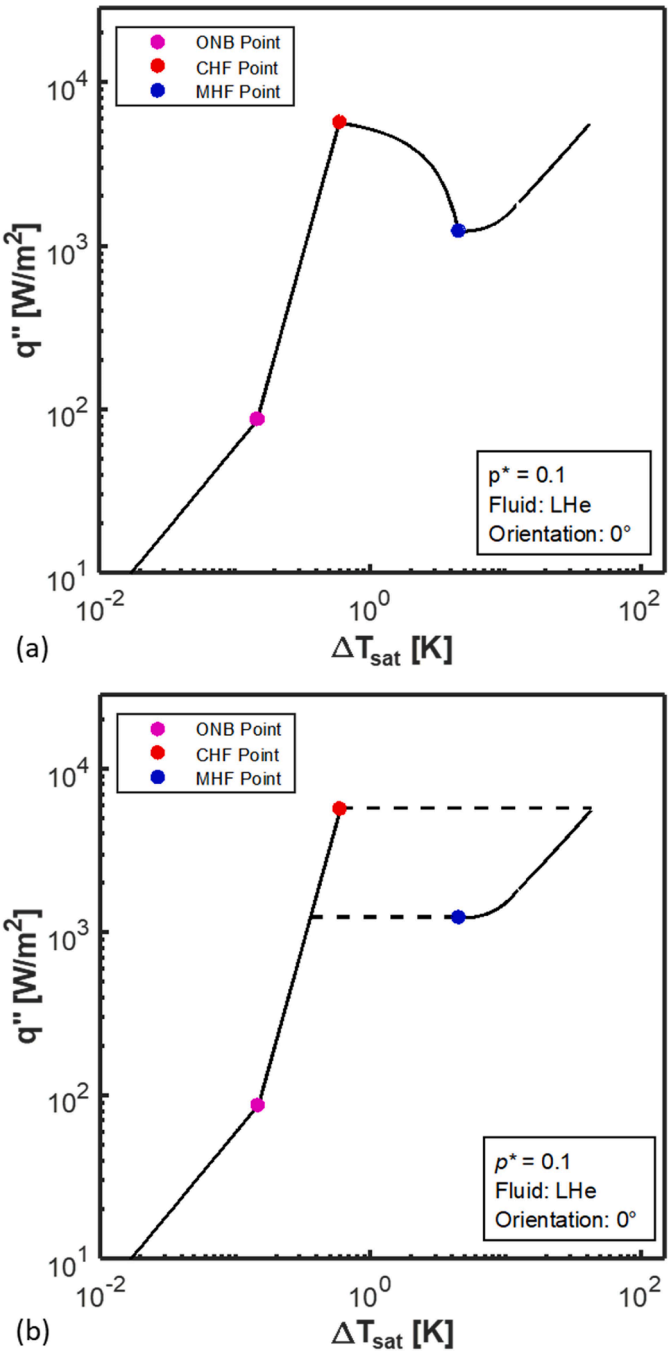

Fig. 7. Comparison of (a) heat-flux-controlled (b) temperature-controlled boiling curve predictions.

controlled boiling curve, respectively, both for LHe at a reduced pressure of $p^* = 0.1$. Both curves were generated using the same correlations discussed earlier, but a key difference stands out: the heat-flux-controlled curve, Fig. 7 (a), does not include the TB regime, whereas the temperature-controlled curve, Fig. 7 (b), does. Other than the TB regime, both curves are identical. Since the primary goal of the present study is to illustrate construction of a complete, continuous boiling curve, all presented boiling curves are shown including TB.

4.2. Validity range and limitations of the new methodology

In the current methodology, all correlations except for $T_{w,min}$ and q''_{min} are independent of the material of the heating surface. As discussed in our prior correlation studies, absence of the surface material effects is rooted entirely in lack of availability of cryogen data needed to incorporate this effect. For this reason, the present methodology is intended for "baseline" prediction of the complete boiling curve. This baseline methodology encompasses: (i) heating surfaces constructed only from copper (material used in most cryogenic pool boiling experiments), (ii) saturated pool boiling, and (iii) terrestrial gravity. It is important to emphasize that we are planning to account for effects of heater size, material, surface roughness, subcooling, and reduced gravity after generating a new, more extensive database, pending experiments we intend to perform both in terrestrial gravity and in reduced gravity (aboard parabolic flight aircraft).

The primary inputs for our baseline methodology are (i) cryogen, (ii) surface orientation angle, (iii) pressure, and (iv) heat flux. For instance, Fig. 8 illustrates the complete saturated pool boiling curve predicted for

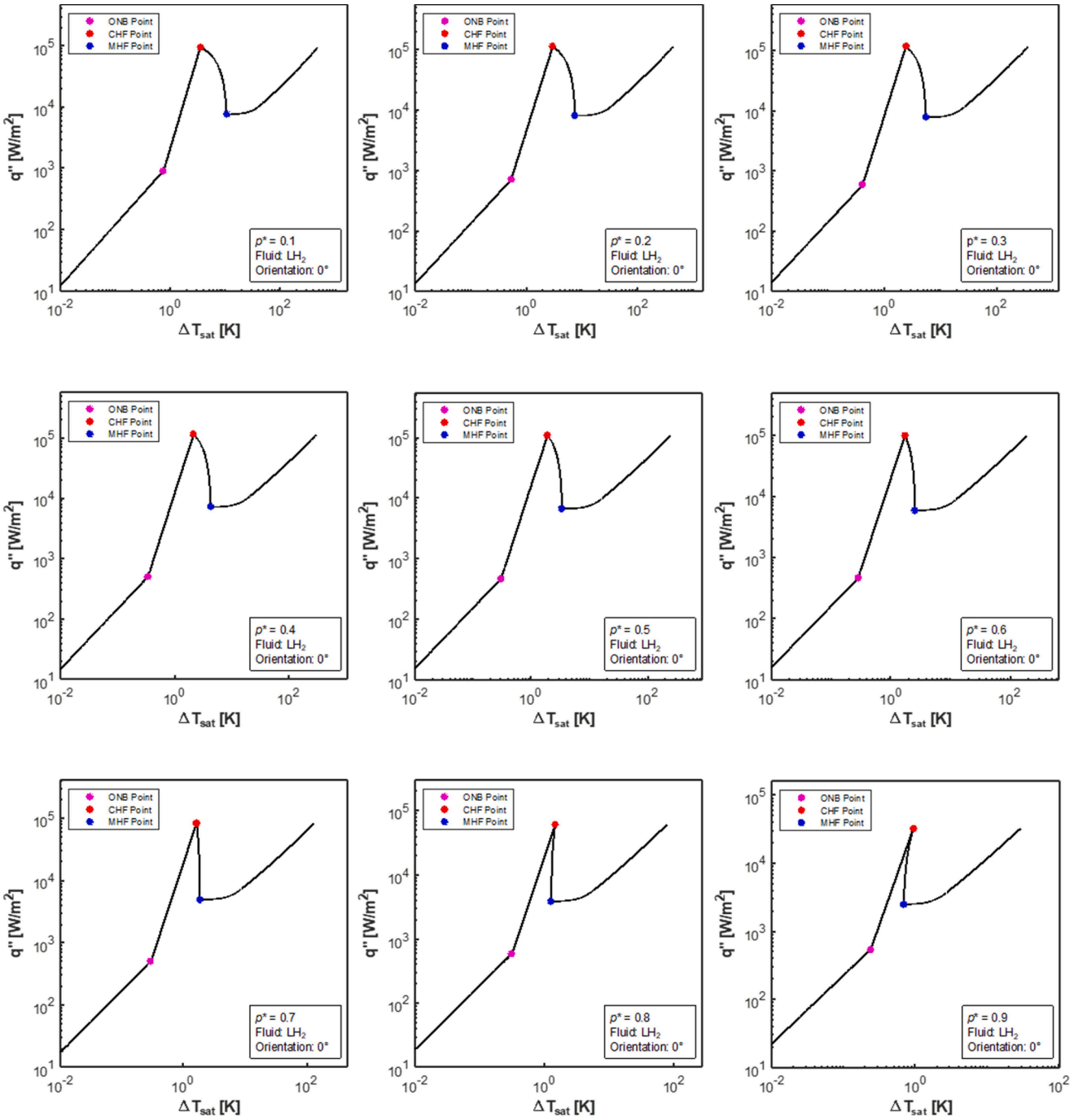

Fig. 8. Predicted continuous boiling curves for LH_2 for reduced pressures from p* = 0.1 to 0.9.

LH_2 over a horizontal copper surface at reduced pressures ranging from $p^* = 0.1$ to 0.9. The figure clearly shows that, as the pressure increases, both $\Delta T_{sat,min}$ and $\Delta T_{sat,CHF}$ shift to the left (i.e., to lower values). However, $\Delta T_{sat,min}$ shows greater sensitivity to pressure as compared to $\Delta T_{sat,CHF}$, which is more clearly seen in Fig. 9 for LHe. Consequently, $\Delta T_{sat,min}$ and $\Delta T_{sat,CHF}$ merge together at very high pressures, thereby compressing the TB region, which is well aligned with the experimental findings of Deev et al. [26].

In Fig. 9, LHe predictions for $\Delta T_{sat,min}$ and $\Delta T_{sat,CHF}$ are plotted against reduced pressure. Fig. 9 (a) also compares predictions to the experimental results of Deev et al.. Notice how Deev et al.'s results show $\Delta T_{sat,min}$ and $\Delta T_{sat,CHF}$ completely merging with one another at $p^* = 0.96$, very close to the critical point. Interestingly, predictions of $\Delta T_{sat,min}$ are precisely aligned with Deev et al.'s data. However, the predicted values of $\Delta T_{sat,CHF}$ exceed the data at very high pressures, causing the predicted $\Delta T_{sat,min}$ and $\Delta T_{sat,CHF}$ to intersect at $p^* = 0.88$, which clearly points to an upper pressure limit for validity of the present methodology. This limit will be addressed in greater detail below. While data for other cryogens at high pressures are scarce, the predictions for LH_2, Fig. 9 (b), and LN_2, Fig. 9 (c), exhibit trends like those for LHe, demonstrating effectiveness of the new methodology across different cryogens.

An interesting observation from Fig. 8 is behavior of the TB region with increasing pressure. The slope of the TB curve steepens with rising pressure and eventually becomes vertical at a certain threshold ($p^* = 0.75$ for LH_2 and LN_2, and 0.88 for LHe); this is where $\Delta T_{sat,min}$ equals $\Delta T_{sat,CHF}$. Above the threshold pressure, the slope of the TB curve turns positive, which seems to contradict known pool boiling curve trends from the literature, suggesting the existence of afore-mentioned upper pressure limit for validity of the new methodology. While the individual correlations for different boiling regimes are valid and usable at higher pressures, the appearance of positive slope for the TB region above the pressure thresholds, shows combining the correlations to construct a continuous boiling curve should be limited to pressures below $p^* = 0.75$.

4.3. *Effects of pressure and orientation angle on continuous pool boiling curve*

In the previous section, Fig. 8 illustrated the effect of pressure variation on the continuous boiling curve for LH_2 and, along with Fig. 9, provided insights into the validity range of the new methodology with respect to pressure. In this section, we extend the discussion to examine the combined effects of pressure and orientation angle on predictive performance. For instance, in Fig. 10, the variations in orientation angle for LHe are analyzed for three different reduced pressures: $p^* = 0.1$, 0.4, and 0.7, representing to low, intermediate, and high pressures. The figure shows a similar trend for both the NC and FB regions with respect to surface orientation, which aligns with existing literature for such buoyancy-driven regimes.

The effect of orientation angle is very noticeable for the NC region and both q''_{ONB} and $\Delta T_{sat,ONB}$. In the NC region, the buoyancy-driven motion and the alignment of the heated surface with gravity strongly influence the heat transfer performance, with vertical orientation ($\theta = 90°$) producing the best performance, followed slightly by horizontal upward-facing orientation ($\theta = 0°$), and more appreciably by horizontal downward-facing orientation ($\theta = 180°$). However, the orientation effect greatly diminishes in the NB regions, where the heat transfer is dominated by formation and detachment of vapor bubbles, which completely dwarf any buoyancy effects. These observations are supported by experimental findings of Tadrist et al. [33], who reported that the effect of orientation on $\Delta T_{sat,ONB}$ is minimal from 0° to 135°, but $\Delta T_{sat,ONB}$ decreases significantly as the orientation approaches 180°. Additionally, they noted that $\Delta T_{sat,ONB}$ decreases with increasing saturation temperature, which is also evident from Fig. 10 in terms of increasing saturation pressure.

It is important to note that our comprehensive review of published work showed that researchers present conflicting views on the effect of

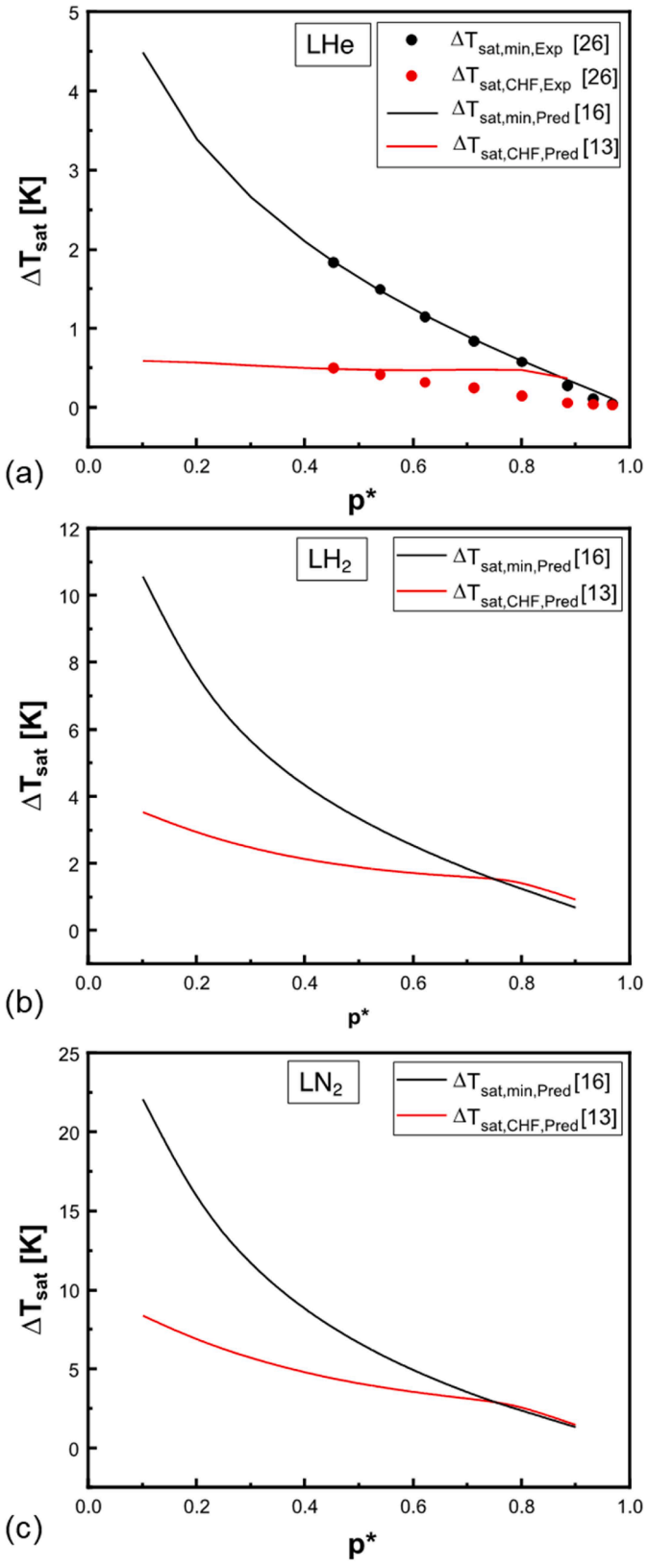

Fig. 9. CHF and MHF superheat predictions versus reduced pressure for (a) LHe (along with experimental data), (b) LH_2, and (c) LN_2.

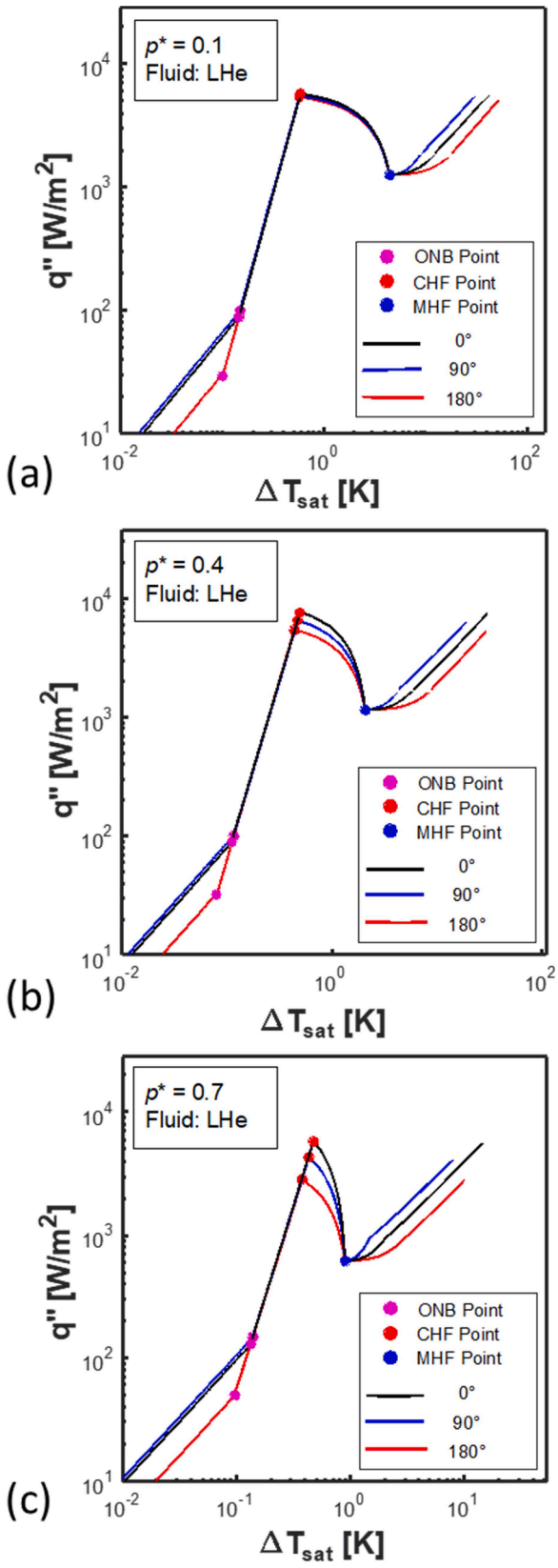

Fig. 10. Effects of orientation angle on continuous boiling curve for LHe at different pressures.

orientation angle in the NB region, with some suggesting this effect is negligible while others argue for its inclusion in correlations. However, our prior correlation for NB [8], which is based on a large database specifically for cryogens, shows the effect of orientation in the NB region is quite miniscule, which is clearly captured in Fig. 10.

Fig. 10 also shows an appreciable influence of orientation on the CHF point, with both q''_{CHF} and $\Delta T_{sat,CHF}$ decreasing with increasing orientation angle, and this trend becoming more pronounced at higher pressures. This trend is consistent with the findings from Patel et al. [15]. On the other hand, according to our prior correlation for the MHF point [16], the orientation effect on q''_{min} and $\Delta T_{sat,min}$ is miniscule. Finally, since the CHF and MHF points serve as "anchors" for the TB region [13], the TB curve follows mostly the same trends relative to orientation as CHF, i.e., the HTC in TB decreases with increasing orientation angle, especially at higher pressures.

Although the model works consistently for all cryogens, presenting results for different fluids helps illustrate its adaptability across cryogens with varying properties. In the earlier sections, we explored key characteristics of our methodology by examining the boiling curves for LH_2 and LHe. Now, we turn our focus to LN_2 to further demonstrate its versatility. In contrast to Fig. 10, which focuses on varying orientation at fixed pressures, Fig. 11 takes a different approach by fixing the orientation angle and examining the effect of pressure on the boiling curve. One of the key observations from Fig. 11 is that, while the HTC in the NC region is strongly influenced by orientation angle (as captured in Fig. 10), its dependence on pressure for a given orientation angle is miniscule.

However, in other regions of the boiling curve, pressure plays a more substantial role. Increasing the pressure causes a horizontal shift in the boiling curve to the left, reducing temperatures of all the boiling curve's transition points: $\Delta T_{sat,ONB}$, $\Delta T_{sat,CHF}$, and $\Delta T_{sat,min}$. Moreover, increasing pressure leads to a decrease in q''_{ONB}, while both q''_{CHF} and $q''_{\min}$ first increase with pressure up to a certain point (around $p^* = 0.35$) before beginning to decrease. This behavior is well-documented in the literature, e.g., Patel et al. [15].

Another significant trend observed in Fig. 11 is how the CHF points (at different pressures and orientations) move away from one another as pressure and orientation angle increase. This is evident both horizontally for $\Delta T_{sat,CHF}$ and vertically for q''_{CHF}, particularly at higher orientation angles and pressures. However, the spread among the MHF points remains consistent across all orientations and pressures, indicating that the MHF point follows the same trend with pressure regardless of the surface orientation. This consistency is likely due to the fact that both $\Delta T_{sat,min}$ and $q''_{\min}$ are very weakly dependent on orientation, which is well documented in the literature as discussed in our previous study [16].

Shifting attention to the effect of pressure on the HTC, Fig. 11 shows that, in both the NB and FB regions, the HTC increases with increasing pressure. However, the rate of increase in the HTC becomes less pronounced at higher pressures, particularly in the NB region and, to a lesser extent, the FB region.

4.4. Comparison of continuous pool boiling curves for different cryogens

In the earlier sections, we have thoroughly discussed the key characteristics of the methodology for constructing the complete pool boiling curve, particularly focusing on specific cryogens like LH2, LHe, and LN_2. In this section, the emphasis shifts toward showcasing the boiling curves for other cryogens. For instance, Fig. 12 presents continuous boiling curves for LAr, LO_2, and LCH_4 horizontal upward-facing orientation at three distinct pressures. Overall, the trends in this figure are like those of LH_2, LHe, and LN_2, which were discussed earlier, but with some differences.

One notable trend that is captured in Fig. 12, particularly for cryogens having higher saturation temperatures (LO_2 and LCH_4), is an

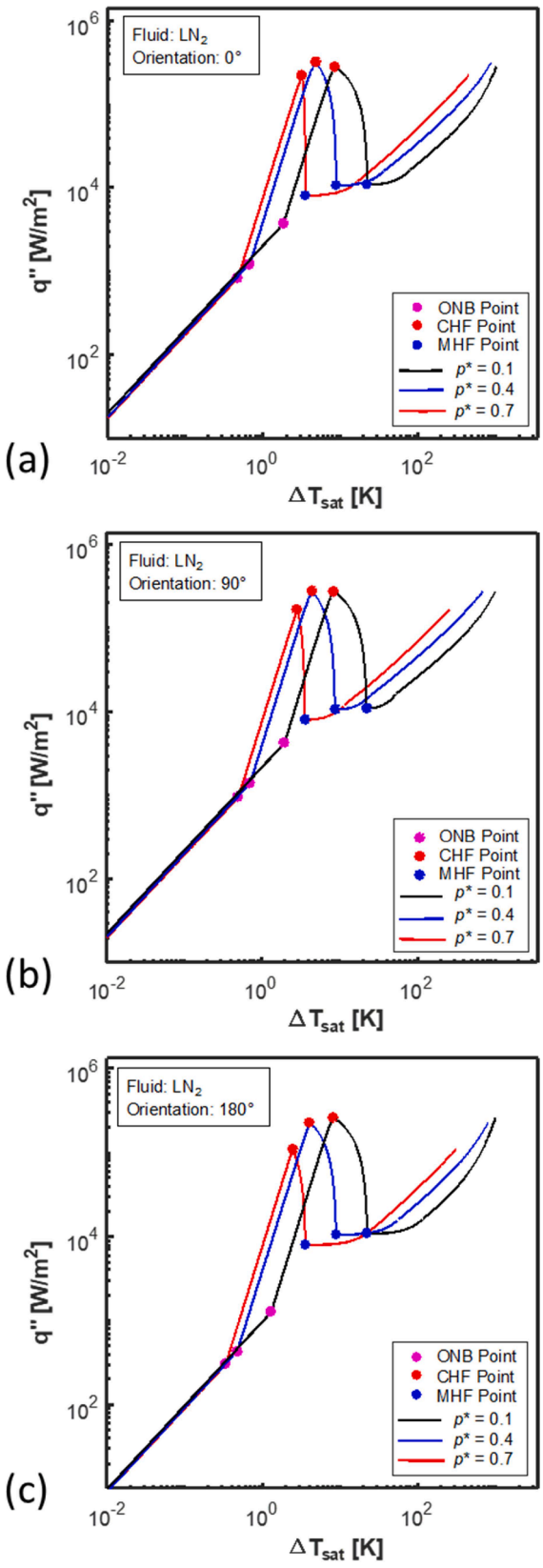

Fig. 11. Effects of pressure on continuous boiling curve of LHe at different orientation angles.

important behavior often observed in experimental pool boiling curves: the decrease in HTC for NB as the CHF point is approached. This behavior is more commonly observed in fluids with higher saturation temperatures, where the reduction in HTC near CHF is quite pronounced. However, the HTC decline is almost nonexistent for very low saturation temperature cryogens like LHe and LH_2. Another notable trend that is captured in Fig. 12 is the decrease in HTC for TB as the CHF point is approached, especially for the higher saturation temperature cryogens (LO_2 and LCH_4). This realistic capture of important experimentally observed trends is further proof of the effectiveness of the correlations incorporated in the present methodology.

4.5. *Recommendations for future work*

Although the new methodology shows impressive predictive capability for the continuous pool boiling curve across cryogens, there is room for improvement in its applicability range and, therefore, both its robustness and utility. Based on the insights from this study, along with those from our prior correlations' studies, the following important tasks are identified for future work:

i. *Improving Prediction of the ONB Point:* Published ONB data are both very sparce and plagued by high measurement uncertainty (mostly because of very low values of corresponding heat flux and wall superheat). This is why the present methodology uses the intersection of the NC and NB curves to predict this point. It is recommended that future experiments be conducted using precise instrumentation to develop a database for multiple cryogens that is of sufficient size to enable developing a new correlation for ONB, similar in accuracy to those available for CHF and MHF.
ii. *Extending Applicability to Higher Pressures*: Currently, our methodology is recommended for use up to a reduced pressure of $p^* = 0.75$. Future work, both experimental and correlation-based, should aim to extend its applicability to near-critical pressure, providing a more comprehensive range of use.
iii. *Incorporating Subcooling Effect:* Because of limitation of the correlations used, the present methodology is only valid for saturated pool boiling. Future experiments should be conducted to address the influence of subcooling for different cryogens. This will enable modifying the present correlations for this effect, which is crucial for many practical applications involving cryogens.
iv. *Accounting for* Heater Size, *Material, and Surface Roughness:* Another crucial missing aspect in our methodology is the ability to account for the effects of heater size, material properties, and surface roughness. This shortfall is the outcome of lack of availability of data for different surface sizes, roughness, and materials. Therefore, it is recommended that future work be conducted using several heater sizes, roughnesses, and surface materials having drastically different thermal properties.
v. *Accounting for Reduced Gravity*: While the current methodology shows excellent predictions for terrestrial gravity, there are several important space-related technologies demanding similar understanding for reduced gravity, especially Lunar and Martian gravities, and microgravity. This is perhaps the most challenging and costly endeavor, requiring performance of experiments in specialized reduced gravity platforms such as parabolic flight aircraft.

It is important to note that achieving the above tasks constitutes the strategy the present authors will be adopting to greatly enhance the applicability of the predictive methodology.

5. Conclusions

The present study is a continuation of a collaborative effort initiated

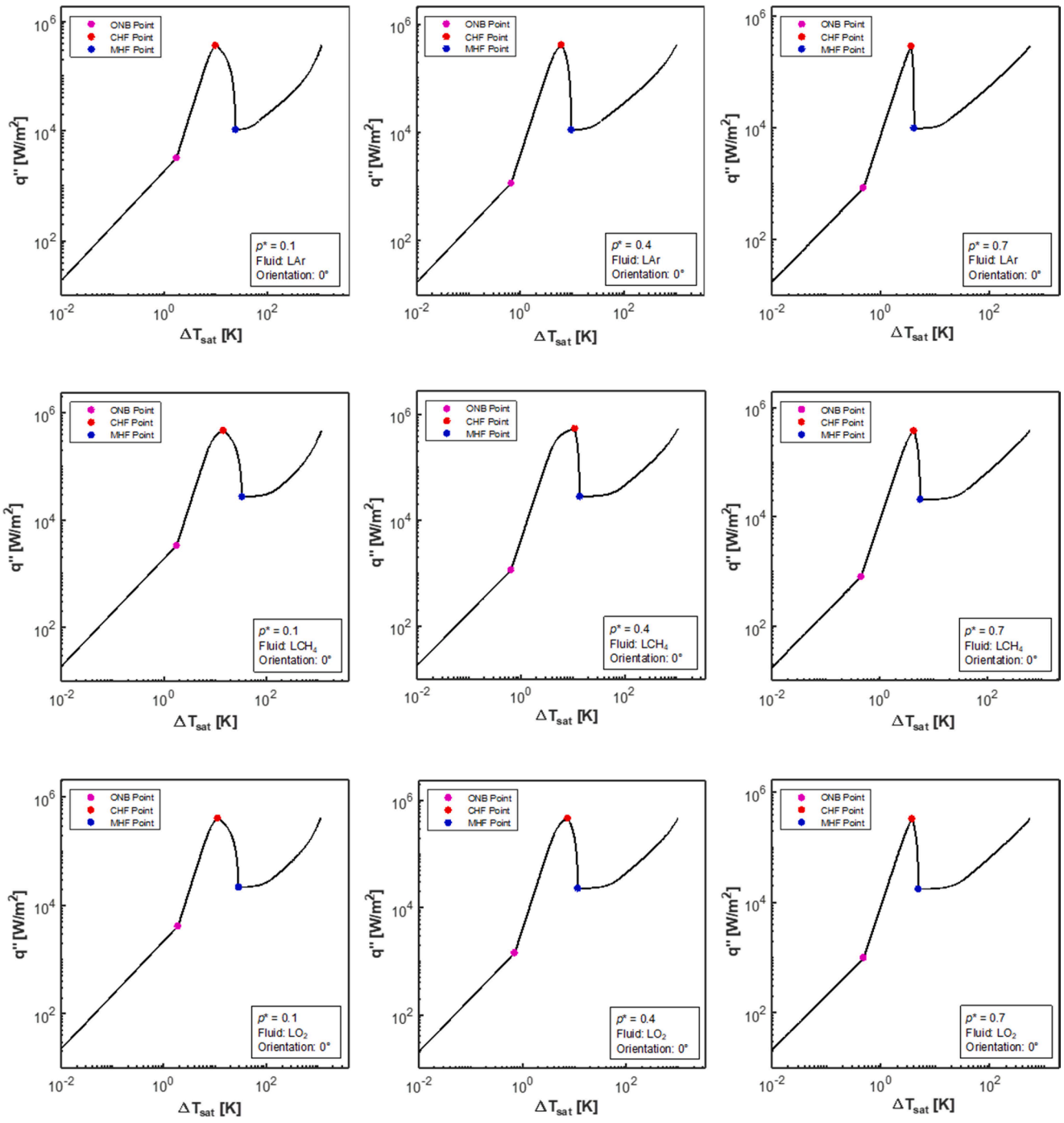

Fig. 12. Predicted boiling curves for LO_2, LCH_4, and LAr at three different pressures.

in 2018 between PU-BTPFL and NASA, aimed at developing predictive correlations for all regimes and transition points of the pool boiling curve for cryogens. To accurately construct a continuous pool boiling curve, careful patching of these correlations is essential to avoid discontinuities between different regimes. This paper carefully detailed the methodology for patching these correlations, utilizing blending functions to ensure a seamless transition across boiling regimes.

Key conclusions drawn from this study are as follows:

I. The new methodology is capable of constructing a continuous boiling curve spanning the entire range of wall superheats and heat fluxes. However, a discontinuity is detected between the FB region and the MHF point. This was corrected by employing a blending function in between.

II. The new pool boiling curve construction methodology shows strong agreement with experimental data for LHe, LH_2, and LN_2 across varying pressure ranges. This robust performance suggests that the methodology would perform well for other cryogens as well, as each regime-specific correlation has already been individually validated.

III. The literature suggests that both $\Delta T_{sat,min}$ and $\Delta T_{sat,CHF}$ decrease with increasing pressure, approaching one another and almost merging together near the critical point. The new methodology also predicts this trend, albeit with the merging occurring a little

earlier than the critical pressure. Overall, the methodology is recommended for pressures up to $p^* = 0.75$.

IV. q''_{CHF} decreases as the orientation angle increases for a given pressure, and this effect is more pronounced at higher pressures. Similarly, for a given orientation, q''_{CHF} first increases to peak value at an intermediate pressure and then decreases. Moreover, the variability in q''_{CHF} increases with increasing orientation angle.

V. In the NC region, the effect of orientation is noticeable while the effect of pressure is almost negligible. Moreover, in both the NB and FB regions, the HTC increases with increasing pressure, however, the rate of increase is less pronounced at high pressures, particularly for the NB region.

VI. The new methodology is capable of predicting the decline in HTC preceding the CHF point, especially for cryogens having higher saturation temperature, such as LO_2 and LCH_4. In contrast, this reduction is nearly absent for cryogens having very low saturation temperatures, reinforcing findings from prior literature.

Author Declaration

We wish to confirm that there are no known conflicts of interest associated with this publication and there has been no significant financial support for this work that could have influenced its outcome.

We confirm that the manuscript has been read and approved by all named authors and that there are no other persons who satisfied the criteria for authorship but are not listed. We further confirm that the order of authors listed in the manuscript has been approved by all of us.

We confirm that we have given due consideration to the protection of intellectual property associated with this work and that there are no impediments to publication, including the timing of publication, with respect to intellectual property. In so doing we confirm that we have followed the regulations of our institutions concerning intellectual property.

We understand that the Corresponding Author is the sole contact for the Editorial process (including Editorial Manager and direct communications with the office). He/she is responsible for communicating with the other authors about progress, submissions of revisions and final approval of proofs. We confirm that we have provided a current, correct email address which is accessible by the Corresponding Author and which has been configured to accept email from mudawar@ecn.purdue.edu

CRediT authorship contribution statement

Faraz Ahmad: Writing – review & editing, Writing – original draft, Validation, Software, Methodology, Investigation, Formal analysis, Data curation, Conceptualization. **Dylan Foster:** Writing – original draft, Validation, Methodology, Investigation, Formal analysis, Data curation, Conceptualization. **Sunjae Kim:** Writing – review & editing, Writing – original draft, Validation, Methodology, Investigation, Conceptualization. **Michael Meyer:** Writing – review & editing, Writing – original draft, Validation, Supervision, Resources, Investigation, Conceptualization. **Jason Hartwig:** Writing – review & editing, Writing – original draft, Validation, Supervision, Resources, Project administration, Methodology, Investigation, Funding acquisition, Conceptualization. **Issam Mudawar:** Writing – review & editing, Writing – original draft, Supervision, Resources, Project administration, Methodology, Investigation, Funding acquisition, Formal analysis, Conceptualization.

Declaration of competing interest

The authors declare the following financial interests/personal relationships which may be considered as potential competing interests: Issam Mudawar reports financial support was provided by NASA. Jason Hartwig reports a relationship with NASA that includes: employment. If there are other authors, they declare that they have no known competing financial interests or personal relationships that could have appeared to influence the work reported in this paper.

Acknowledgments

The authors are grateful for financial support of the National Aeronautics and Space Administration (NASA) Small Business Technology Transfer (STTR) program under a subcontract from MTS Inc. Phase II contract 80NSSC23CA009. We also thank the Fulbright Program for providing a scholarship for the first author.

Data availability

The data that has been used is confidential.

References

[1] NASA Space Technology Mission Directorate, Civil space shortfall rankings, NASA Report, July 23rd, 2024.
[2] T.J. LaClair, I. Mudawar, Thermal transients in a capillary evaporator prior to the initiation of boiling, Int. J. Heat. Mass Transf. 43 (2000) 3937–3952.
[3] G. Liang, I. Mudawar, Pool boiling critical heat flux (CHF) – part 2: assessment of models and correlations, Int. J. Heat. Mass Transf. 117 (2018) 1368–1383.
[4] I. Mudawar, R.A. Houpt, Mass and momentum transport in smooth falling liquid films laminarized at relatively high Reynolds numbers, Int. J. Heat. Mass Transf. 36 (1993) 3437–3448.
[5] T.C. Willingham, I. Mudawar, Channel height effects on forced-convection boiling and critical heat flux from a linear array of discrete heat sources, Int. J. Heat. Mass Transf. 35 (1992) 1865–1880.
[6] C.O. Gersey, I. Mudawar, Effects of heater length and orientation on the trigger mechanism for near-saturated flow boiling critical heat flux - II. Critical heat flux model, Int. J. Heat. Mass Transf. 38 (1995) 643–654.
[7] S. Mukherjee, I. Mudawar, Pumpless loop for narrow channel and micro-channel boiling from vertical surfaces, J. Electron. Packag. 125 (2003) 431–441.
[8] M.T. Meyer, I. Mudawar, C.E. Boyack, C.A. Hale, Single and two-phase cooling with an array of rectangular jets, Int. J. Heat. Mass Transf. 49 (2006) 17–29.
[9] I. Mudawar, T.A. Deiters, A universal approach to predicting temperature response of metallic parts to spray quenching, Int. J. Heat. Mass Transf. 37 (1994) 347–362.
[10] M.K. Sung, I. Mudawar, Single-phase and two-phase heat transfer characteristics of low temperature hybrid micro-channel/micro-jet impingement cooling module, Int. J. Heat. Mass Transf. 51 (2008) 3882–3895.
[11] M.K. Sung, I. Mudawar, Single-phase and two-phase hybrid cooling scheme for high-heat-flux thermal management of defense electronics, J. Electron. Packag. 131 (2009) 021013.
[12] F. Ahmad, S. Kim, M. Meyer, J. Hartwig, I. Mudawar, Saturated nucleate pool boiling of cryogenic fluids: review of databases, assessment of existing models and correlations, and development of new universal correlation, Int. J. Heat. Mass Transf. 231 (2024) 125807.
[13] F. Ahmad, M. Meyer, J. Hartwig, I. Mudawar, Development of new correlations for critical heat flux point wall temperature and transition boiling under steady-state saturated pool boiling of cryogens, Int. J. Heat. Mass Transf. 239 (2025) 126592.
[14] F. Ahmad, M. Meyer, J. Hartwig, I. Mudawar, Saturated pool film boiling of cryogenic fluids: review of databases, assessment of existing models and correlations, and development of new universal correlation, Int. J. Heat. Mass Transf. 235 (2024) 126190.
[15] R. Patel, M. Meyer, J. Hartwig, I. Mudawar, Review of cryogenic pool boiling critical heat flux databases, assessment of models and correlations, and development of new universal correlations, Int. J. Heat. Mass Transf. 190 (2022) 122579.
[16] F. Ahmad, M. Meyer, J. Hartwig, I. Mudawar, Development of new universal correlations for minimum heat flux point for saturated pool boiling of cryogens, Int. J. Heat. Mass Transf. 234 (2024) 126099.
[17] F.P. Incropera, D.P. DeWitt, T.L. Bergman, A.S. Lavine, Fundamentals of Heat and Mass Transfer, Wiley, New York, 1996.
[18] J.R. Lloyd, W.R. Moran, Natural convection adjacent to horizontal surface of various planforms, J Heat Trans 96 (1974) 443–447.
[19] W.H. McAdams, Heat Transmission, McGrow-Hill, 1954.
[20] F.J. Bayley, An analysis of turbulent free-convection heat-transfer, Proc. Inst. Mech. Eng. 169 (1955) 361–370.
[21] E. Radziemska, W.M. Lewandowski, Heat transfer by natural convection from an isothermal downward-facing round plate in unlimited space, Appl. Energy 68 (2001) 347–366.
[22] H. Ogata, W. Nakayama, Heat transfer to subcritical and supercritical helium in centrifugal acceleration fields 1. Free convection regime and boiling regime, Cryogenics. (Guildf) 17 (1977) 461–470.
[23] G.R. Chandratilleke, S. Nishio, H. Ohkubo, Pool boiling heat transfer to saturated liquid helium from coated surface, Cryogenics. (Guildf) 29 (1989) 588–592.
[24] A. Iwamoto, R. Maekawa, T. Mito, J. Yamamoto, Steady state heat transfer characteristics in He I with different surface area, Adv. Cryog. Eng. (1998) 1481–1487.

[25] H. Ogata, H. Mori, Steady state heat transfer in transition boiling of helium on copper surfaces, Cryogenics. (Guildf) 33 (1993) 640–642.
[26] V.I. Deev, V.E. Keilin, I.A. Kovalev, A.K. Kondratenko, V.I. Petrovichev, Nucleate and film pool boiling heat transfer to saturated liquid helium, Cryogenics. (Guildf) 17 (1977) 557–562.
[27] H. Merte, Incipient and Steady Boiling of Liquid Nitrogen and Liquid Hydrogen Under Reduced Gravity, Tech Report, University of Michigan, 1970.
[28] C.R. Class, J.R. DeHaan, M. Piccone, R.B. Cost, Boiling heat transfer to liquid hydrogen from flat surfaces, Adv. Cryog. Eng. 5 (1960) 254–261.
[29] P.J. Marto, J.A. Moulson, M.D. Maynard, Nucleate pool boiling of nitrogen with different surface conditions, J. Heat. Trans. 90 (1968) 437–444.
[30] F.D. Akhmedov, V.A. Grigorev, A.S. Dudkevic, Boiling of nitrogen at pressures from atmospheric to critical, Therm. Eng. 21 (1974) 120–121.
[31] S.P. Ashworth, C. Beduz, J. Mayne, A. Pasek, R.G. Scurlock, Evaluation of a novel enhanced boiling surface in cryogenic liquids, Adv. Cryog. Eng. 35 (1990) 429–435.
[32] B.V Balakin, M.I. Delov, K.V Kutsenko, A.A. Lavrukhin, O.V Zhdaneev, Heat transfer from Ni–W tapes in liquid nitrogen at different orientations in the field of gravity, Cryogenics. (Guildf) 65 (2015) 5–9.
[33] L. Tadrist, H. Combeau, M. Zamoum, M. Kessal, Experimental study of heat transfer at the transition regime between the natural convection and nucleate boiling: Influence of the heated wall tilt angle on the onset of nucleate boiling (ONB) and natural convection (ONC), Int. J. Heat. Mass Transf. 151 (2020) 119388.